Measurements of SOLEIL Insertion Devices using the pulsed wire method

Mathieu VALLÉAU

SYNCHROTRON SOLEIL
Magnetism And Insetion Devices Group

June 6, 2013

Method developped in 1987 at Los Alamos by R. WARREN.

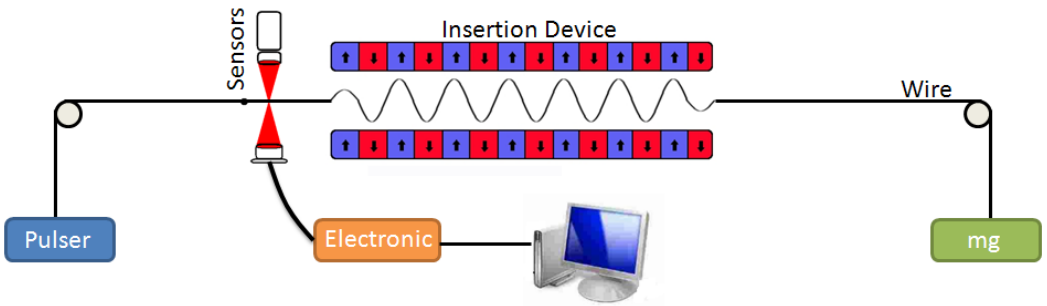

Figure 1: *Global scheme of the method*

ADVANTAGES

- Enables to measure low gap or without lateral access IDs or cryogenic devices
- Short measuring time ($< 8ms$)

DRAWBACKS

- Low signal to noise ratio, leading to a bad accuracy, reproducibility, reliability ...

Current/magnetic field interaction => **Laplace forces** : $d\vec{f}_{Lap} = \vec{I}\ dl \otimes \vec{B}$

R.W. WARREN, New system for Wiggler fabrication and testing, Los Alamos National Lab., 1987
R.W. WARREN, Limitations on the use of the pulsed wire field measuring technique, Nuclear Instruments And Methods, 1988

Wire without rigidity and distortion free propagation.

In the **vertical** plane :

$$\mu \frac{\partial z^2}{\partial t^2} = T \frac{\partial z^2}{\partial s^2} - mg + B_x(s) I(t) \qquad (1)$$

In the **horizontal** plane :

$$\mu \frac{\partial x^2}{\partial t^2} = T \frac{\partial x^2}{\partial s^2} + B_z(s) I(t) \qquad (2)$$

With :

1. μ the wire density
2. T, the mechanical strenght
3. $B(s)\ I(t)$, Laplace forces
4. $m\ g$, the wire weight
5. I_0 : current pulse amplitude
6. Δ_t : current pulse delay
7. c : wave propagation speed

1. **First integral measurements** : $\Delta t \approx 20\mu s$

$$x(t) = -\frac{I_0 \Delta t}{2\mu c} \int_0^{vt} B_z(s) ds \quad and \quad z(t) = -\frac{I_0 \Delta t}{2\mu c} \int_0^{vt} B_x(s) ds \qquad (3)$$

2. **Second integral measurements** : $\Delta t \approx 8ms$

$$x(t) = -\frac{I_0}{2\mu c^2} \int \int B_z(s) ds ds' \quad and \quad z(t) = -\frac{I_0}{2\mu c^2} \int \int B_x(s) ds ds' \qquad (4)$$

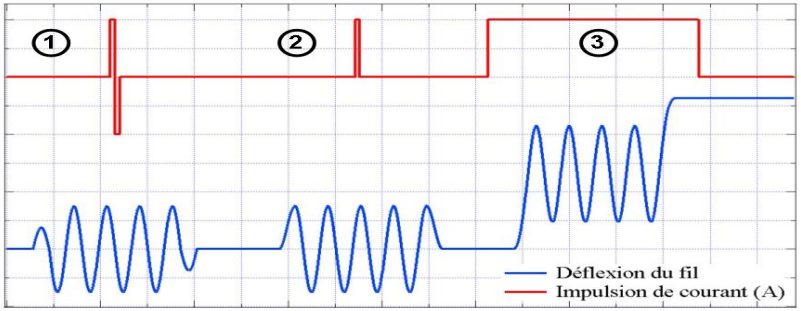

Figure 2: *Pulse shape for the different measurements (magnetic field, angle and trajectory)*

$$c = \sqrt{\frac{T}{\mu}} \tag{5}$$

The increase in speed goes along with a degradation to the signal-to-noise ratio.

The method suffers from low signal to noise ratio (SNR). Two ways of improvements :

- Improve the wire vibrations :
  - Specific wire
  - Adapted pulser
- Improve the sensitivity of the sensors :
  - To be less sensitive to electronic noise
  - To be less sensitive to optical noise

However no averaging is needed, datas are available in single shot ($\approx 10\ ms$)

6 m long wire stretched between 2 points on the magnetic axis of the ID.

Wire	$\mu\ \rho$
AlSi	$4.64\ 10^{-12}$
CuBe	$4.66\ 10^{-11}$
W	$5.05\ 10^{-10}$

- High ϕ : more current but more dispersion
  125 μ**m diameter choosen**
- High T : less distorsions and less sag
  28 N **mechanical strenght applied**
  c $\approx$ 350 $m.s^{-1}$

$$Sag : \frac{g\ L_u^2}{8\ c^2} \approx 40\ \mu m \qquad (6)$$

Optimized wire : low $\mu\ \rho$ product
- Low μ : large displacements
- Low ρ : more current

Tungsten wire is used in our case

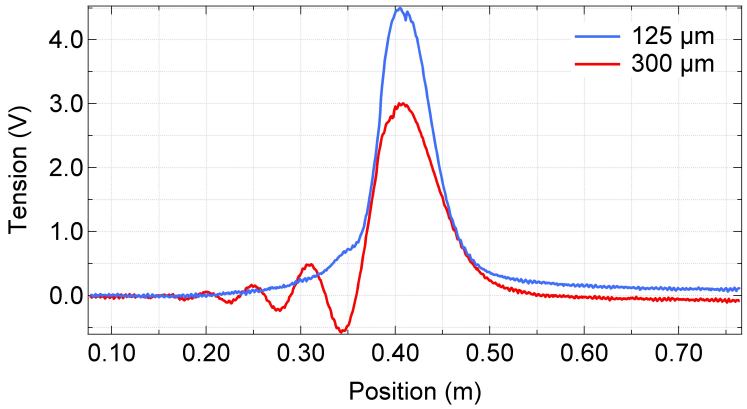

Figure 3: *Distortions between W wires*

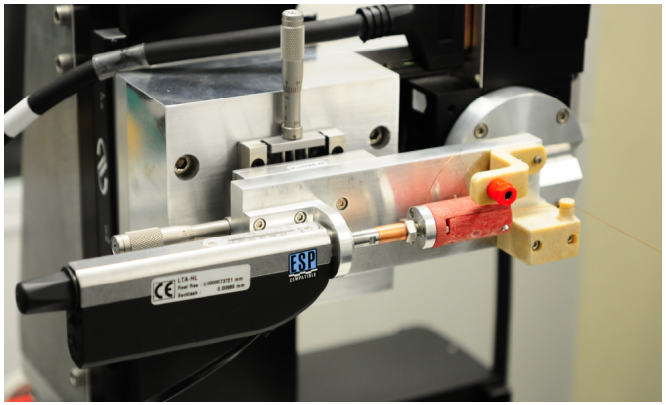

Figure 4: *Left side fixing point with actuator to stretch the wire*

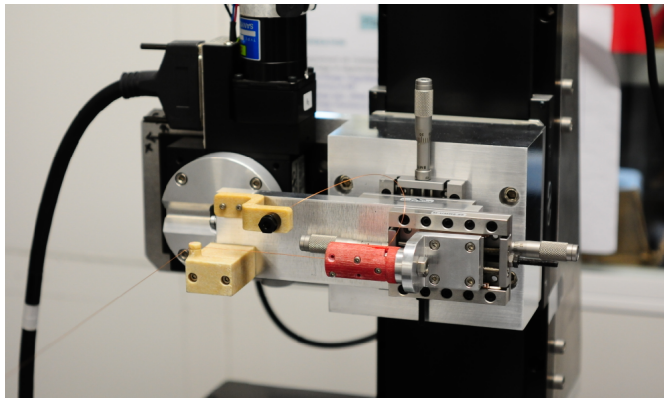

Figure 5: *Right side fixing point.*

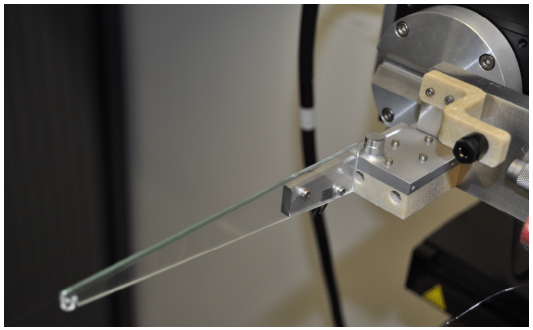

Figure 6: *Oil dampers*

Damping reflexions both sides using oil

A.A. VARFOLOMEEV, Detailled analysis of pulsed wire method accuracy, Nuclear Instruments And Methods in Physics Research, 1997

A photodiode delivers a current proportional to the wire position

- Emitter : laser diode @ 400 nm (low noise)
- Receiver : photodiode BPX65rt (high speed)
- Home made electronic to :
  - convert current into voltage
  - amplify the signal
  - adapt the signal to the DAQ (substractor, impedance adaptation...)

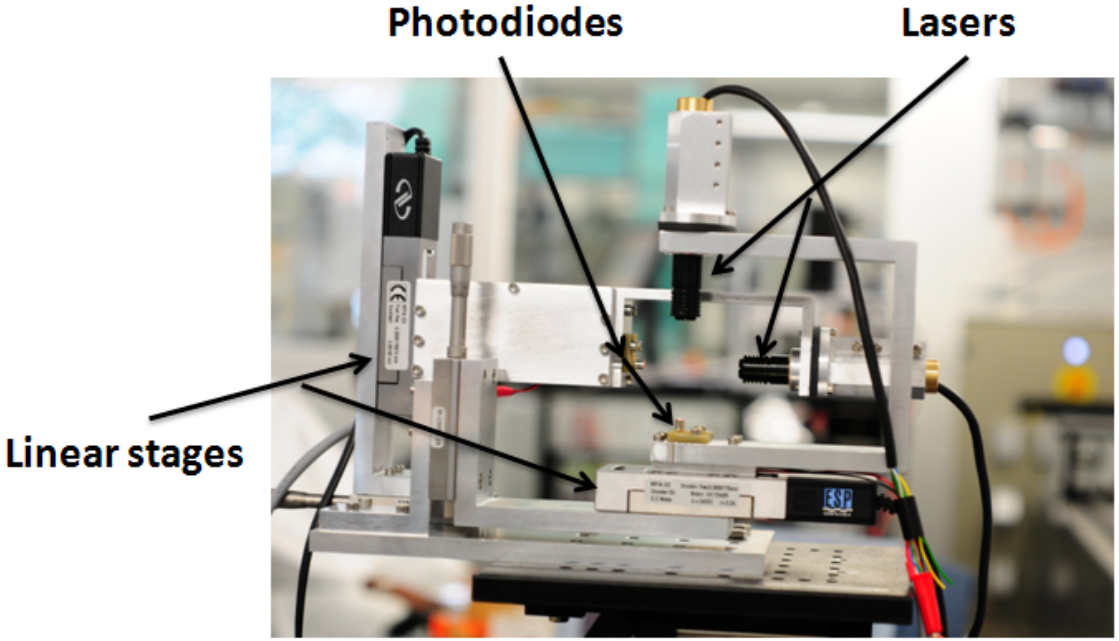

Figure 7: *Horizontal and vertical sensors composed of a laser in front of a photodiode. Sensors are installed on linear stage for calibration.*

- Sensors output voltage : $\pm 18\ V$.
- Acquisition card input voltage : $\pm 10\ V$.
- Calibration needed to calculate $I1$ and $I2$.
- $> 3.5\ V/\mu m$.

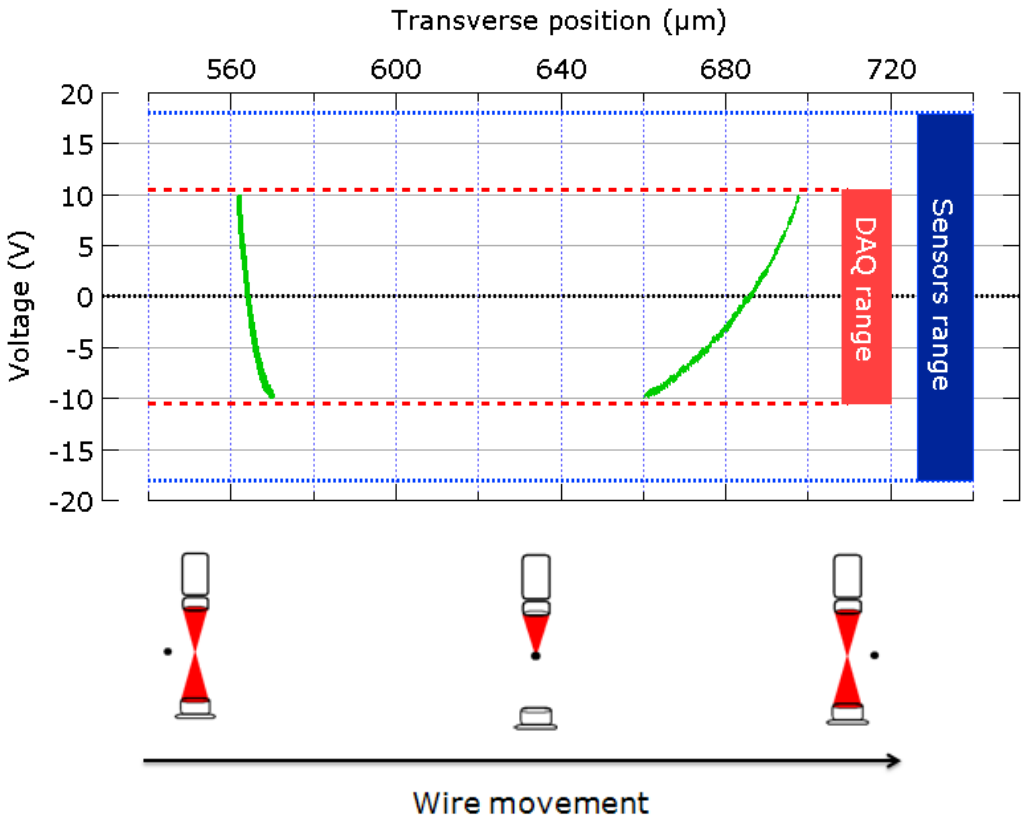

Figure 8: *Calibration curve of the sensors while the wire crosses the laser*

Maximixing the slope :

- Reduces electronic noise regarding to usefull signal ($\approx$ 250 mV)
- Reduces optical noise regarding to usefull signal ($\approx$ 20 mV)

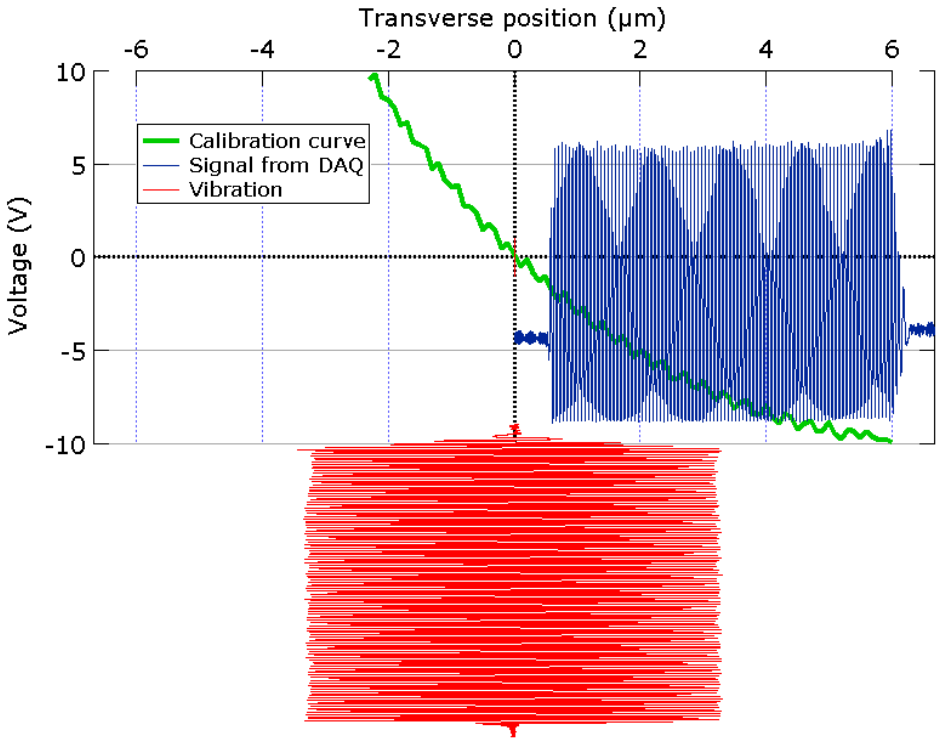

Figure 9: *Calibration curve of the sensors*

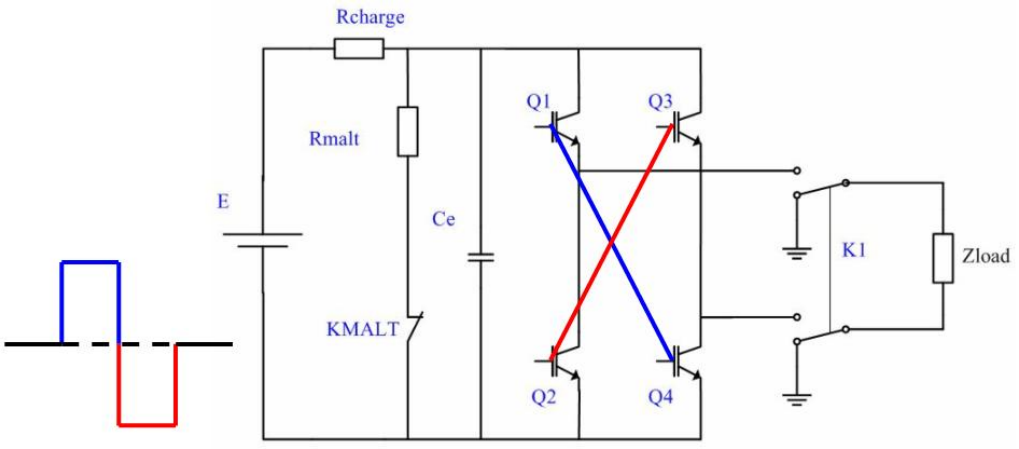

Figure 10: *Scheme of the pulser*

- Home made pulser
- Max. voltage : 300 V
- Max current : 10 A
- Rise time : 0.2 μs
- Decrease for 10 ms pulses : 4.5%
- Bipolar **Positive**/**Negative**

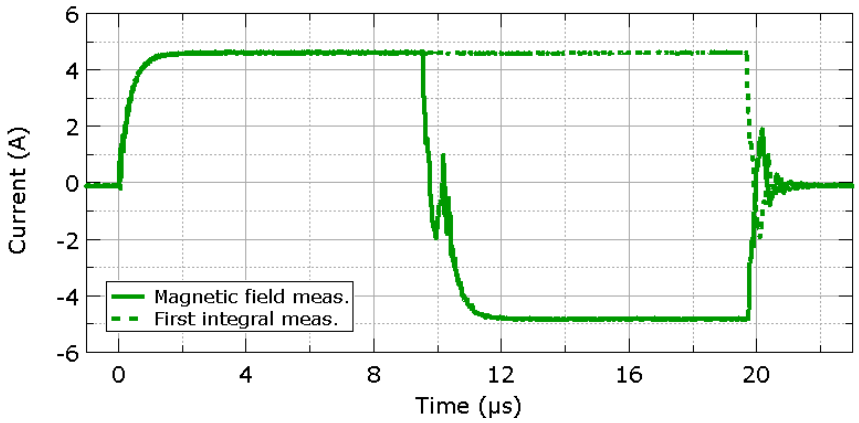

Figure 11: *Currents delivered by pulser for magnetic field and first integral measurements.*

Both sides : 4 strain gages in full bridge :

- monitor the wire heating during long pulses
- control the mechanical strenght

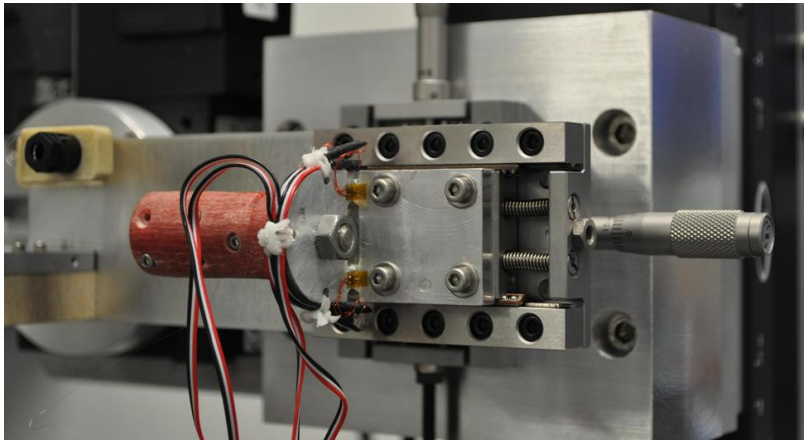

Figure 12: *Strain gages glued on fixed point*

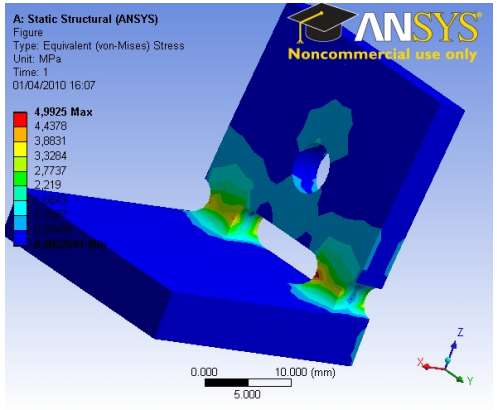

Figure 13: *Deformation simulated via ANSYS under a 10 N strenght*

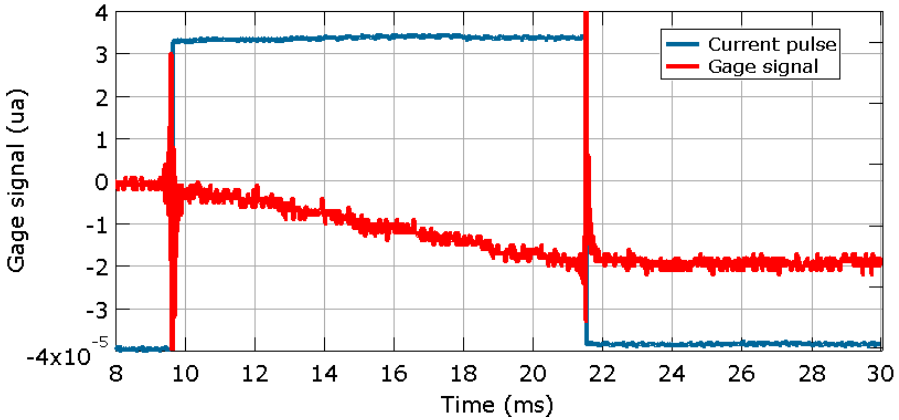

Figure 14: *Gage measurements during long pulses.*

Wiener filtering : "a priori" knowledge of the signal to estimate

Learning phase :

Magnetic field **square**, current pulse **sinus**

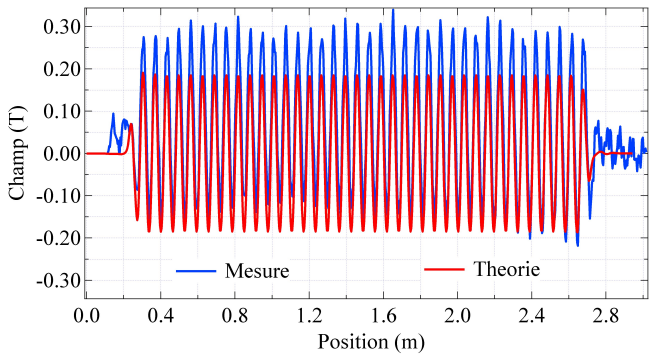

Figure 15: *Learning phase*

Filtering phase :

Magnetic field **sinus**, current pulse **square**

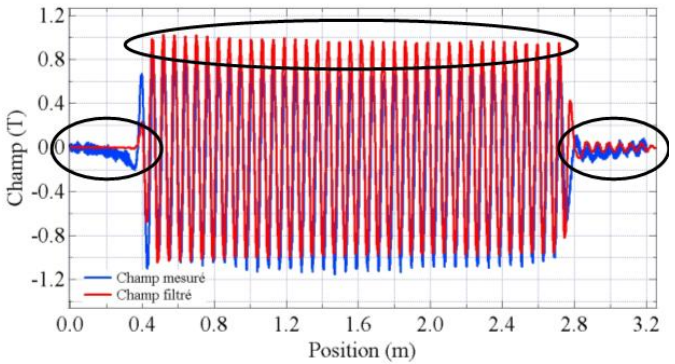

Figure 16: *Filtering phase*

$$w_{mc} = R^{-1}p \tag{7}$$

w_{mc} filtering coefficients matrix, R auto-cor. matrix, p inter-cor. matrix
=> **efficient method, but in this particular case, it is penalized by the low amplitude of the sinusoïdal current pulse (80 mA) leading to wrong trajectory .**

F. MARTEAU, M. CORLIER, C. FAYE ,O. MARCOUILLE, Improvements of the pulsed wire method to measure undulators, Transaction on Applied Superconductivity, 2000

- Sag correction

$$B = B_0 \left[\cosh\left(\frac{2\pi}{\lambda_0} z\right) \cos\left(\frac{2\pi}{\lambda_0} s\right) - \sinh\left(\frac{2\pi}{\lambda_0} z\right) \sin\left(\frac{2\pi}{\lambda_0} s\right) \right] \tag{8}$$

- Non linear correction using the calibration curve

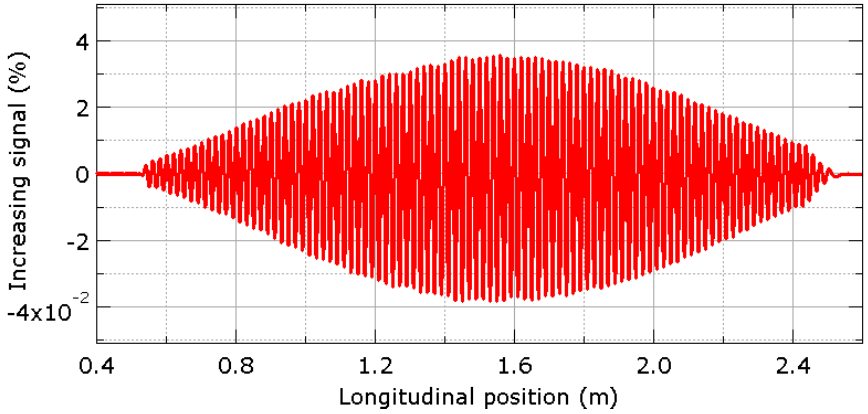

Figure 17: *Signal increase due to wire sag*

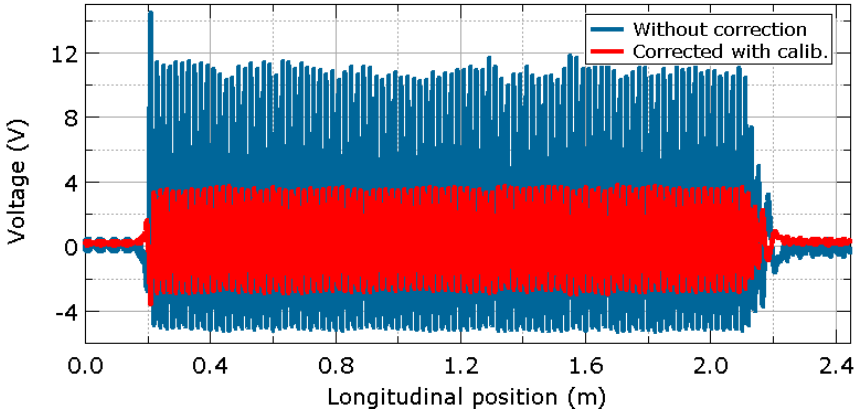

Figure 18: *Effect of the non-linear correction using the calibration curve*

A.A. VARFOLOMEEV et al., Further development of the pulsed wire technique for magnetic field and focusing strength measurements in long undulators, Nucl. Instr. And Meth. In Phys. Res, A407, 43-47, 1998

	HU36	*HU42*	*HU44*	*HU52*	*HU60*	*HU64*	*HU80*
Nb.	1	1	2	2	2	1	3
Period [mm]	36	42	44	52	60	64	80
Nb. periods	44	38	36	30	26	24	19
H. field [T]	0.51	0.45	0.45	0.5	0.57	0.64	0.7
V. field [T]	0.74	0.67	0.68	0.74	0.83	0.82	0.92
Aperiodic						Yes	Yes
Energy [keV]	2-10	1-8	1-8	0.5-6	0.1-4	0.1-4	0.04-1.6

Table 1: *12 APPLE II IDs already installed in the storage ring.*

	U18	*U20*	*U20*	*U24*	*WSV50*	*HU640*	*HU256*	*EMPHU65*
Nb.	1	5	2	1	1	1	3	1
Period [mm]	18	20	20	24	50	640	256	65
Nb. periods	106	98	98	81	38	14	12	26
H. field [T]						0.09	0.28	0.24
V. field [T]	1.15	0.97	1.08	0.82	2.1	0.11	0.44	0.24
Aperiodic							Oui	
Energy [keV]	1.5-30	3-18	3-18	3-18	10-50	0.005-0.04	0.01-1	5-17

Table 2: *Cryogenic, in-vacuum and elctromagnetic IDs already installed in the storage ring.*

APPLE II devices

- Gap range : 15.5 mm to 240 mm
- Phase shift : ϕ : $\pm\frac{\lambda_0}{2}$ *mm*
- Four polarization modes :

1. **Linear Horizontal** for $\phi = 0$ mm
2. **Linear Vertical** for $\phi = \frac{\lambda_0}{2}$ mm
3. **Helicoïdal** for parallel movements (incl. ciruclar)
4. **Linear Tilted** for anti-parallel movements

$$\vec{B} = \left[B_x cos\left(\frac{2\pi S}{\lambda_0} + \Phi\right); B_z cos\left(\frac{2\pi S}{\lambda_0}\right); 0\right]$$

$$\lambda_r = \frac{\lambda_0}{2\gamma^2}\left(1 + \frac{K_x^2}{2} + \frac{K_z^2}{2} + \gamma^2\theta^2\right) \quad (10)$$

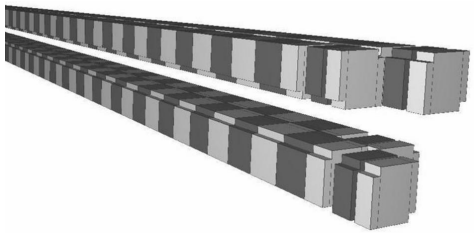

Figure 19: *RADIA model of an APPLE II undulator*

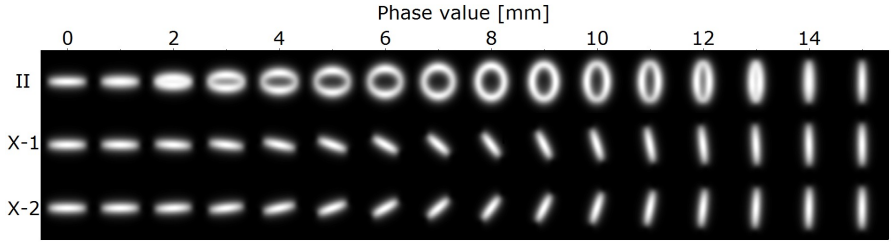

Figure 20: *Polarization produced by a 30 mm period APPLE II undulator*

O. CHUBAR et al., A three-dimensional magnetostatic computer code for insertion devices, Journal of Synchrotron Radiation, 5 481-484, 1998

ID magnetic parameters :

Type : APPLE II
Period : 60 mm
Peak field : 0.83 T (V) 0.57 T (H)
$K_z = 4.65$, $K_x = 3.2$

Second integral meas. parameters :

I_0 **:** 0.5 A
Δ_t **:** 10 ms
c : 300 $m.s^{-1}$

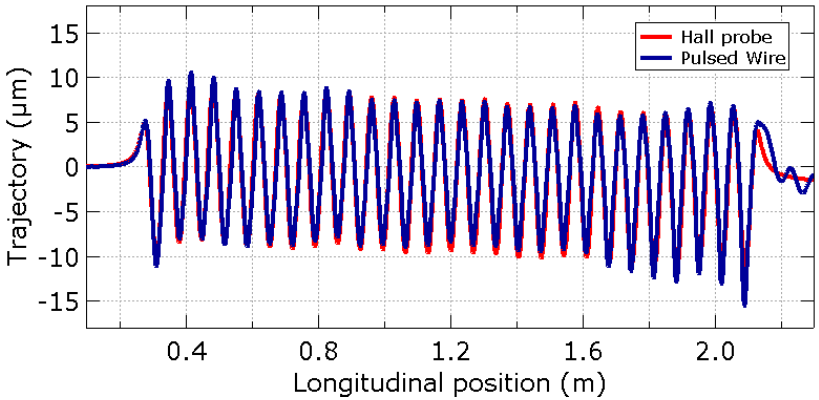

Figure 21: *Horizontal trajectories.*

$$\Delta_{I2x} = 0\ \mu\text{m}$$

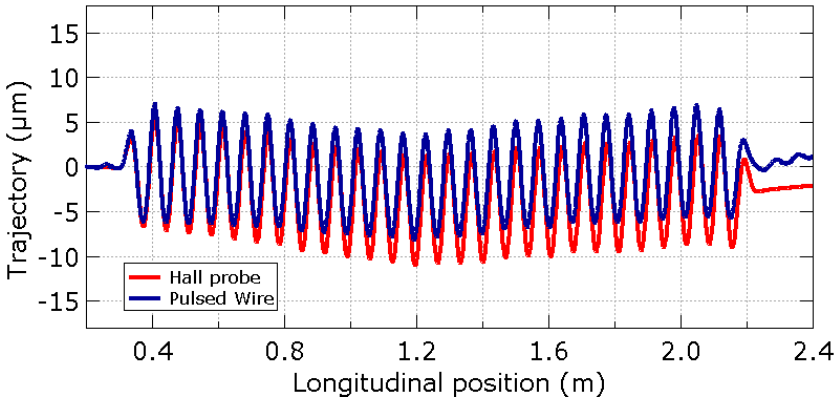

Figure 22: *Vertical trajectories.*

$$\Delta_{I2z} \approx 3\ \mu\text{m}$$

M.-E. COUPRIE et al., First SOLEIL insertion devices are ready to produce photons, Nucl. Instr. And Meth. in Phys. Res., A575 33-37, 2007

ID magnetic parameters :

Type : APPLE II
Period : 60 mm
Peak field : 0.83 T (V) 0.57 T (H)

Second integral meas. parameters :

I_0 **:** 0.5 A
Δ_t **:** 10 ms
c : 300 $m.s^{-1}$

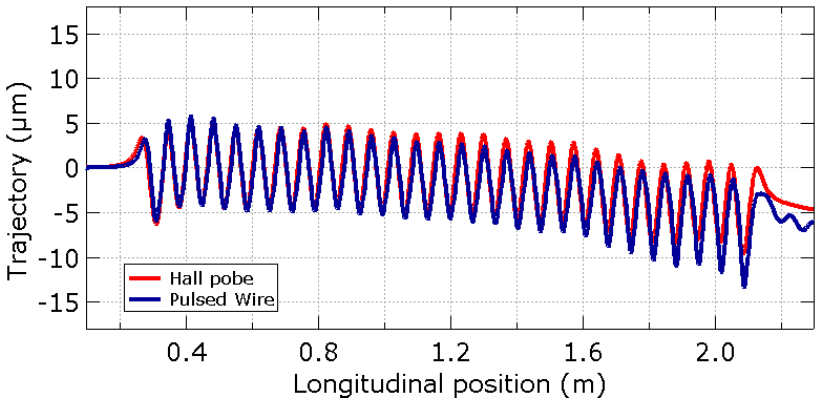

Figure 23: *Horizontal trajectories.*

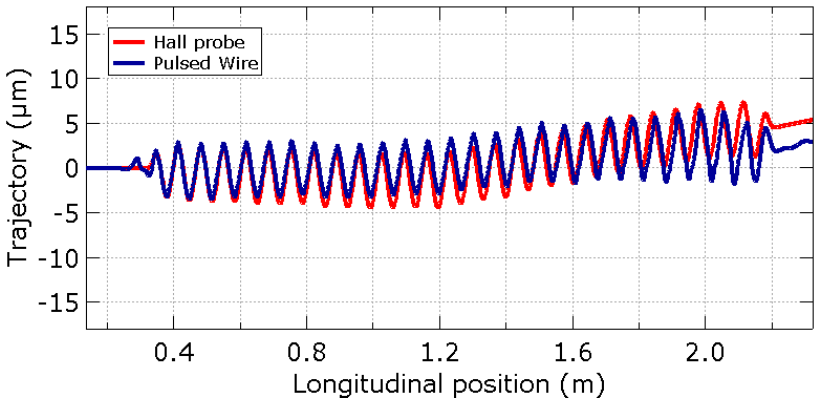

Figure 24: *Vertical trajectories.*

$$\Delta_{I2x} \approx 1.5\ \mu m \qquad \Delta_{I2z} \approx 3\ \mu m$$

Differences $<$ 3 μm in both planes for second integral measurements in every polarizations.

M.-E. COUPRIE et al., First SOLEIL insertion devices are ready to produce photons, Nucl. Instr. And Meth. in Phys. Res., A575 33-37, 2007

Planar in-vacuum undulators

- Gap range : 5.5 mm to 30 mm
- Only Linear Horizontal polarization

$$\vec{B} = \left[0; B_z cos\left(\frac{2\pi S}{\lambda_0}\right); 0\right] \quad (11)$$

$$\lambda_r = \frac{\lambda_0}{2\gamma^2}\left(1 + \frac{K_z^2}{2} + \gamma^2\theta^2\right) \quad (12)$$

Figure 25: *In-vacuum undulator without vacuum vessel*

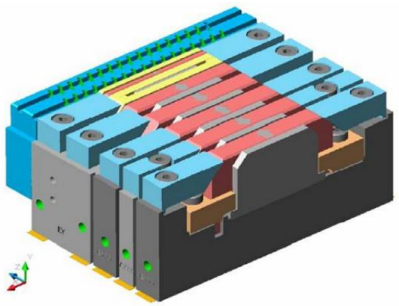

Figure 26: *Endkeepers of a planar in-vacuum undulator*

ID magnetic parameters :

Type : Cryogenic
Period : 18 mm
Peak field : 1.05 T - 1.16 T (V)
$K_z = 1.95$

Second integral meas. parameters :

I_0 **:** 5 A
Δ_t **:** 10 ms
c : 330 $m.s^{-1}$

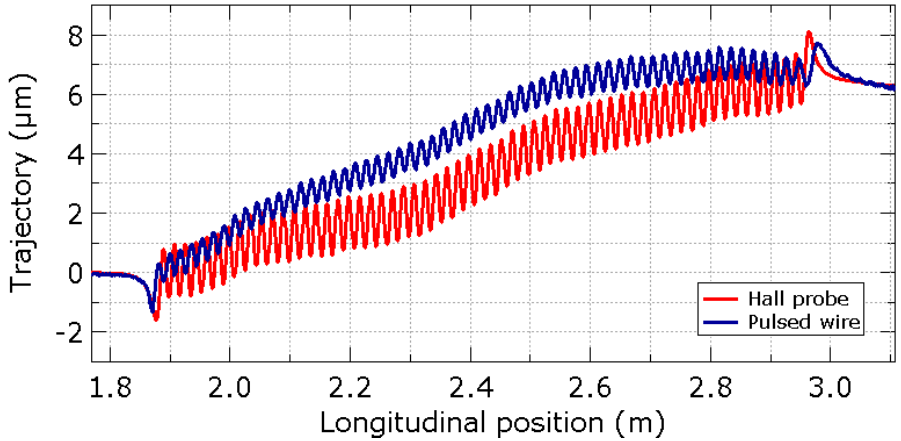

Figure 27: *Horizontal trajectories*

First full-scale PrFeB cryogenic undulator installed in a storage ring.

Differences $<$ 3 μm for second integral measurements.

C. BENABDERRAHMANE et al., $Nd_2Fe_{14}B$ and $Pr_2Fe_{14}B$ magnets characterisation and modelling for Cryogenic Permanent Magnet Undulator applications, Nucl. Instr. And Meth. , A669, 1, 2011

C. BENABDERRAHMANE et al., Development of a $Pr_2Fe_{14}B$ cryogenic undulator at SOLEIL, Proceedings of IPAC, 2010

ID magnetic parameters :

Type : In-vacuum wiggler
Period : 50 mm
Peak field : 2.1 T (V)
$K_z = 9.8$

Second integral meas. parameters :

I_0 **:** 0.5 A
Δ_t **:** 10 ms
c : 300 $m.s^{-1}$

Figure 28: *The wiggler with compensation springs to counter magnetic forces.*

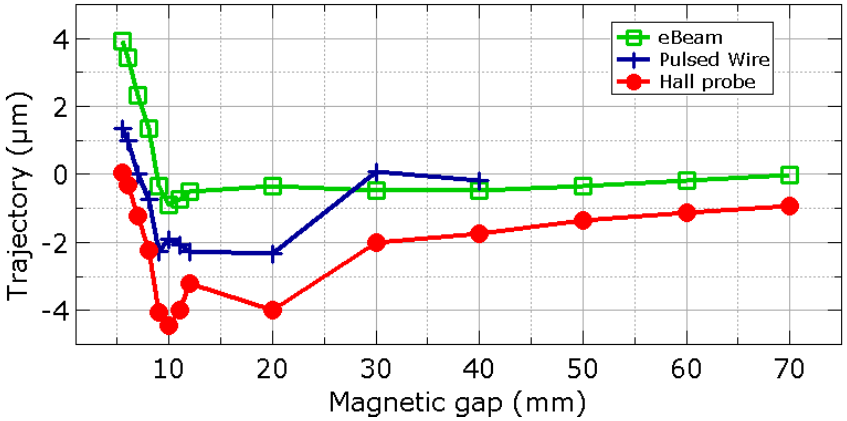

Figure 29: *Second integral values versus magnetic gap measured with Hall probe and pulsed wire in comparison with on-beam measurements.*

Differences $<$ 3 μm for second integral measurements.

O. MARCOUILLÉ et al., An in-vacuum wiggler WSV50 for producting hard X-rays at SOLEIL, Proceedings of EPAC, 2008

ID magnetic parameters :

Type : In-vacuum
Period : 20 mm
Peak field : 0.96 T (V)
$K_z = 1.8$

Second integral meas. parameters :

I_0 **:** 1 A
Δ_t **:** 8 ms
c : 350 $m.s^{-1}$

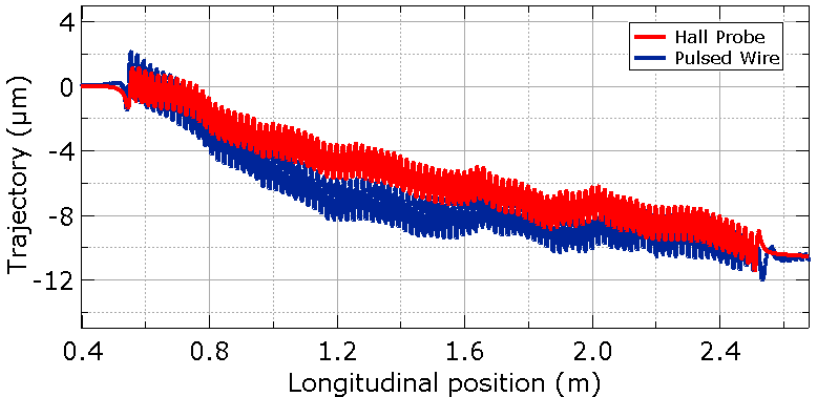

Figure 30: *Horizontal trajectories.*

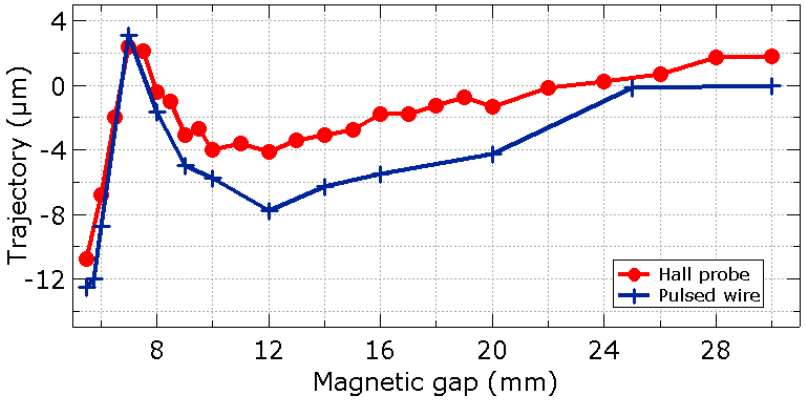

Figure 31: *Second integral values versus magnetic gap.*

Differences $<$ 4 μm for second integral measurements.

M.-E. COUPRIE et al., Development and installation of Insertion Devices at SOLEIL, Proceedings of PAC, 2009

ID magnetic parameters :

Type : In-vacuum
Period : 20 mm
Peak field : 0.96 T (V)

First integral meas. parameters :

I_0 **:** 8.75 A
Δ_t **:** 20 μs
c : 350 $m.s^{-1}$

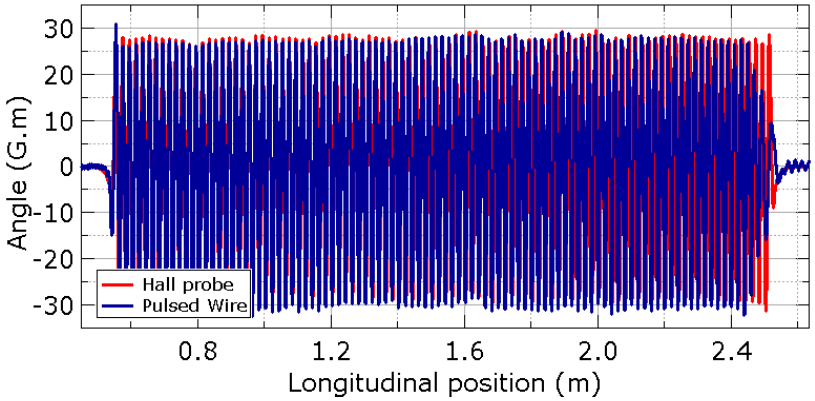

Figure 32: *Horizontal angles.*

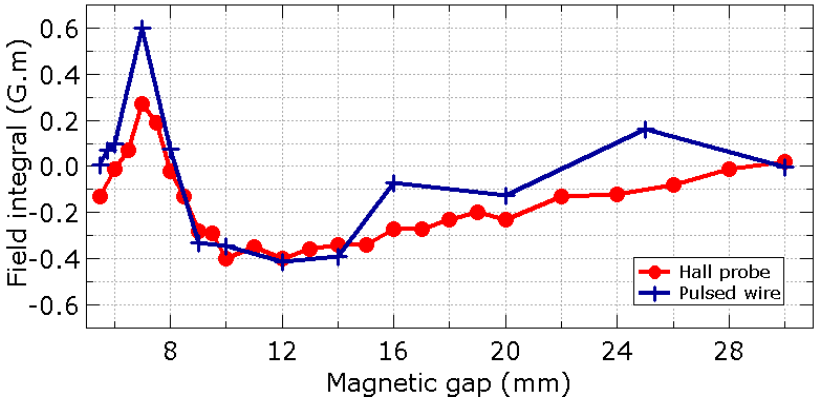

Figure 33: *First integral values versus magnetic gap.*

Differences $<$ 0.3 $G.m$ **for first integral measurements.**

M.-E. COUPRIE et al., Development and installation of Insertion Devices at SOLEIL, Proceedings of PAC, 2009

ID magnetic parameters :

Type : In-vacuum
Period : 20 mm
Peak field : 0.96 T (V)

Magnetic field meas. parameters :

I_0 : 8.75 A
Δ_t : 20 μs
c : 350 $m.s^{-1}$

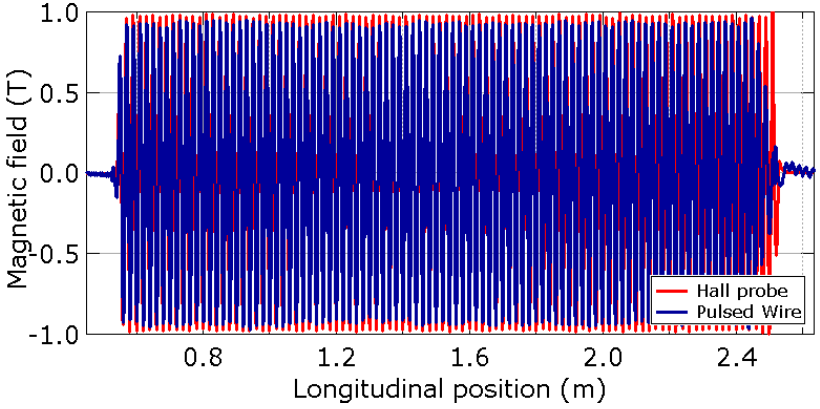

Figure 34: *Vertical magnetic field.*

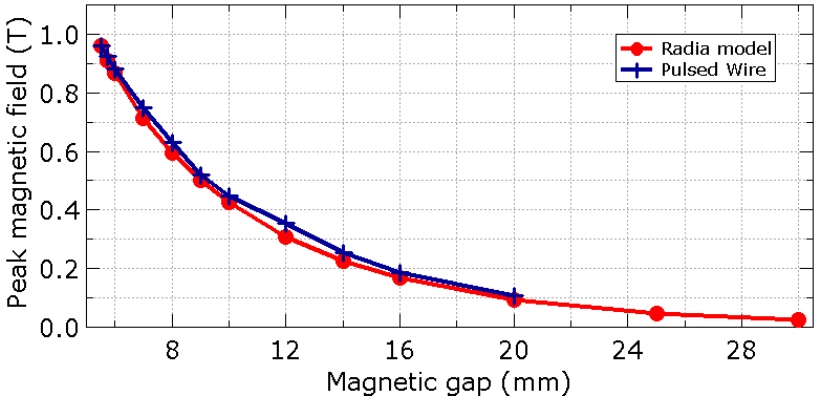

Figure 35: *Vertical peak magnetic field versus gap value.*

Magnetic field measurements using Pulsed Wire are normalized in amplitude thanks to Hall probe measuremements at minimal gap.

M.-E. COUPRIE et al., Development and installation of Insertion Devices at SOLEIL, Proceedings of PAC, 2009

ID magnetic parameters :

Type : In-vacuum
Period : 20 mm
Peak field : 0.96 T (V)

Magnetic field meas. parameters :

I_0 : 8.75 A
Δ_t : 20 μs
c : 350 $m.s^{-1}$

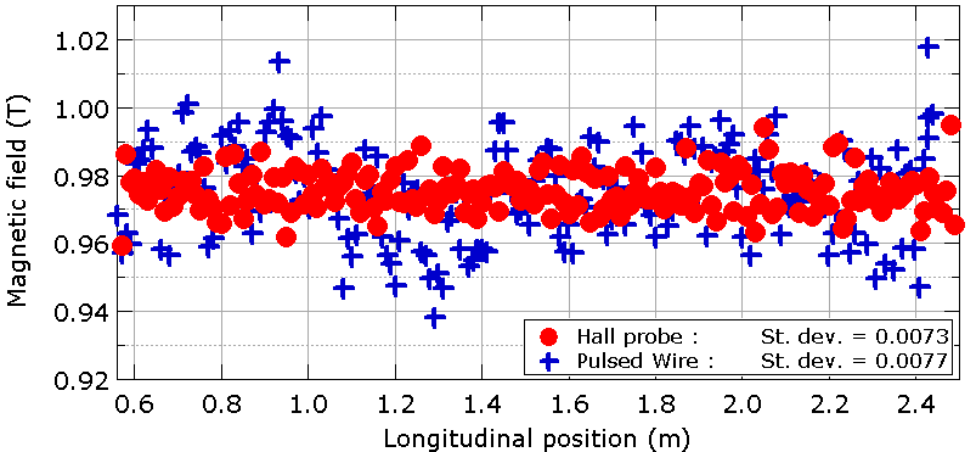

Figure 36: *Vertical magnetic field absolute peak values.*

B2E phase error calculation : 4.5 ° (Hall probe) vs 15 ° (Pulsed Wire)

M.-E. COUPRIE et al., Development and installation of Insertion Devices at SOLEIL, Proceedings of PAC, 2009

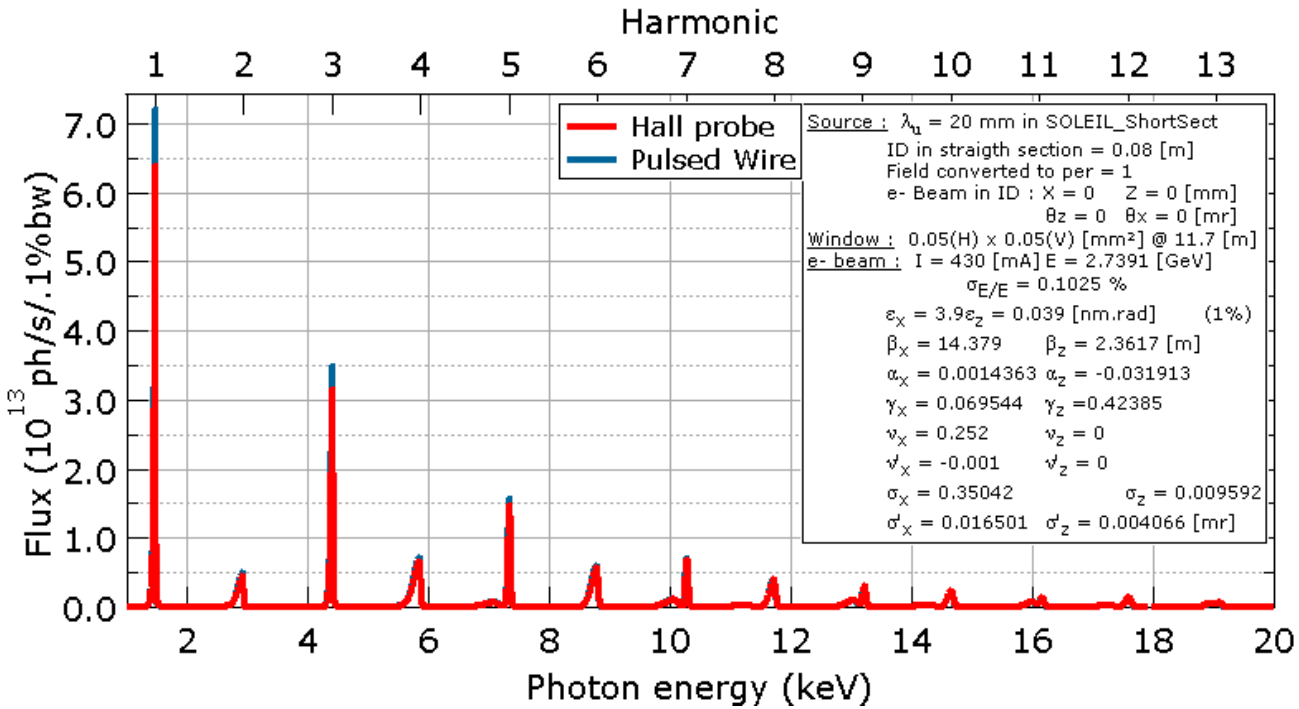

Figure 37: *Spectra computed using PWM magnetic field measurement (blue) and Hall probe measurement (red).*

- Calculation performed with SRW using the "convert to periodic" function
- Pulsed Wire magnetic field is normalized in amplitude to scale the energy

M.-E. COUPRIE et al., Development and installation of Insertion Devices at SOLEIL, Proceedings of PAC, 2009

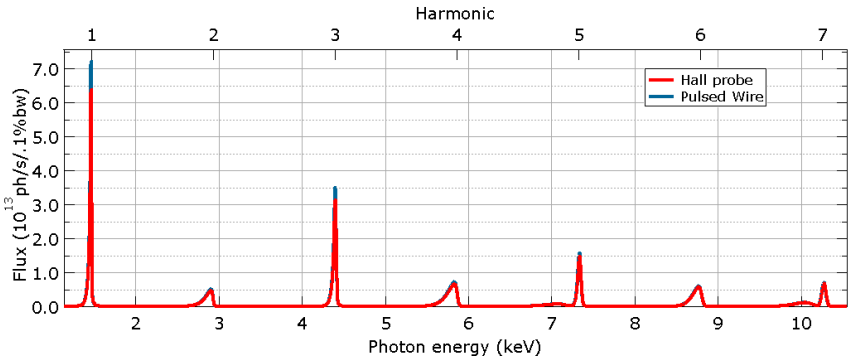

Figure 38: *Spectra computed using Pulsed Wire (blue) and Hall probe measurements (red) from H1 to H7.*

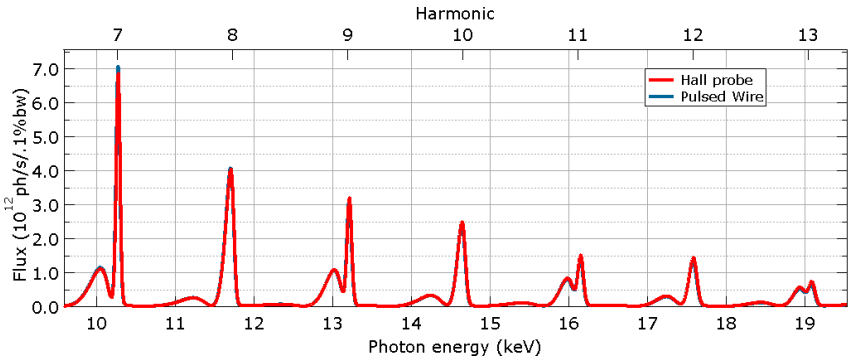

Figure 39: *Spectra computed using Pulsed Wire (blue) and Hall probe measurements (red) from H7 to H13.*

M.-E. COUPRIE et al., Development and installation of Insertion Devices at SOLEIL, Proceedings of PAC, 2009

- The pulsed wire method has been tested on several undulators (APPLE II and in-vacuum) such as a wiggler in all polarizations.
- Period range : 18 mm to 60 mm
- Magnetic field range : 0 to 2.1 T
- Magnetic lenght : 1.6 m to 2 m

All the measurements are available with a single shot, no averaging is needed.

- All the PWM measurements have been compared to Hall probe ones, even sometimes with ebeam ones.
- Second integral :
  - $\approx$ 3 μm compared to Hall probe measurements or ebeam ones
  - reproducibility : 0.2 μm.
- First integral :
  - $\approx$ 0.3 G.m compared to Rotating Coil data
  - reproducibility : 0.1 G.m
  - 3 periods are missing
- Magnetic field : spectrum calculated with SRW is very close to the one calculated from Hall probe measurements using the "convert to periodic" function. However, 3 periods are missing and corrections are necessary (dispersion) to calculate the phase error => still to improve.